we would have to accept a very long path length of $L = 85$ pc and a low density of $\langle n_H \rangle = 6\,cm^{-3}$. On the other hand, if we adopt the canonical path length, we must increase the ionization rate to $\zeta = 1.2 \times 10^{-15}\,s^{-1}$. Given the evidence pointing to a short path length, and the fact that ζ is essentially unconstrained in diffuse clouds, we consider the higher ionization rate to be the more likely explanation. A higher value of ζ for diffuse clouds may also find some support from considerations of the abundance of the OH molecule[26]. A more detailed discussion of the ζ Persei line of sight, as well as other observations of H_3^+ in diffuse clouds, will be presented elsewhere.

The high value of ζ suggested by the CRYRING measurements and the ζ Persei observations can be reconciled with the lower ionization rate in dense clouds by postulating the existence of a large flux of low-energy cosmic rays that can penetrate diffuse clouds but not dense clouds. Such a cosmic-ray flux would bring the models and observations of H_3^+ into agreement, but would also have far-reaching implications for the chemistry and physics of interstellar clouds. From a chemical perspective, a higher value of ζ would proportionately increase the number densities of oxygen compounds such as OH, as well as affecting the relative abundances of deuterium-bearing molecules. The high number density of H_3^+ in diffuse clouds would also increase the rate of proton-transfer reactions, which play the key role in the formation of complex molecules in dense clouds, but which have been considered relatively unimportant in diffuse clouds. From a physical perspective, a higher cosmic-ray ionization rate represents an additional heating source for interstellar gas, and could have a significant impact on the thermal balance of the warm neutral medium[27]. Further observations of H_3^+, H_2 and C^+ in lines of sight to other diffuse clouds are needed to determine if the ζ Persei line of sight is unusual, or whether a large, low-energy cosmic ray flux indeed pervades our galaxy. □

Received 19 November 2002; accepted 17 February 2003; doi:10.1038/nature01498.

1. Herbst, E. & Klemperer, W. The formation and depletion of molecules in dense interstellar clouds. *Astrophys. J.* **185,** 505–534 (1973).
2. Watson, W. D. The rate of formation of interstellar molecules by ion-molecule reactions. *Astrophys. J.* **183,** L17–L20 (1973).
3. Geballe, T. R. & Oka, T. Detection of H_3^+ in interstellar space. *Nature* **384,** 334–335 (1996).
4. McCall, B. J., Geballe, T. R., Hinkle, K. H. & Oka, T. Observations of H_3^+ in dense molecular clouds. *Astrophys. J.* **522,** 338–348 (1999).
5. McCall, B. J., Geballe, T. R., Hinkle, K. H. & Oka, T. Detection of H_3^+ in the diffuse interstellar medium toward Cygnus OB2 No. 12. *Science* **279,** 1910–1913 (1998).
6. Geballe, T. R., McCall, B. J., Hinkle, K. H. & Oka, T. Detection of H_3^+ in the diffuse interstellar medium: the Galactic center and Cygnus OB2 Number 12. *Astrophys. J.* **510,** 251–257 (1999).
7. McCall, B. J. *et al.* Observations of H_3^+ in the diffuse interstellar medium. *Astrophys. J.* **567,** 391–406 (2002).
8. Larsson, M. Experimental studies of the dissociative recombination of H_3^+. *Phil. Trans. R. Soc. Lond. A* **358,** 2433–2444 (2000).
9. Oka, T. Help!!! Theory for H_3^+ recombination badly needed. in *Dissociative Recombination of Molecular Ions with Electrons* (ed. Guberman, S. L.) (Kluwer Academic/Plenum, New York, in the press).
10. Guberman, S. L. Dissociative recombination without a curve crossing. *Phys. Rev. A* **49,** R4277–R4280 (1994).
11. Orel, A. E., Schneider, I. F. & Suzor-Weiner, A. Dissociative recombination of H_3^+: progress in theory. *Phil. Trans. R. Soc. Lond. A* **358,** 2445–2456 (2000).
12. Schneider, I. F., Orel, A. E. & Suzor-Weiner, A. Channel mixing effects in the dissociative recombination of H_3^+ with slow electrons. *Phys. Rev. Lett.* **85,** 3785–3788 (2000).
13. Sundström, G. *et al.* Destruction rate of H_3^+ by low-energy electrons measured in a storage ring experiment. *Science* **263,** 785–787 (1994).
14. Jensen, M. J. *et al.* Dissociative recombination and excitation of H_3^+. *Phys. Rev. A* **63,** 052701 (2001).
15. Tanabe, T., *et al.* in *Dissociative Recombination: Theory, Experiment and Applications* Vol. IV (eds Larsson, M., Mitchell, J. B. A. & Schneider, I. F.) 170–179 (World Scientific, Singapore, 2000).
16. Kokoouline, V., Greene, C. H. & Esry, B. D. Mechanism for the destruction of H_3^+ by electron impact. *Nature* **412,** 891–894 (2001).
17. Kokoouline, V. & Greene, C. H. Theory of dissociative recombination of D_{3h} triatomic ions, applied to H_3^+. *Phys. Rev. Lett.* (in the press).
18. Strasser, D. *et al.* Breakup dynamics and the isotope effect in H_3^+ and D_3^+ dissociative recombination. *Phys. Rev. A* **66,** 032719 (2002).
19. Kreckel, H. *et al.* Vibrational and rotational cooling of H_3^+. *Phys. Rev. A* **66,** 052509 (2002).
20. Larsson, M., *et al.* Studies of dissociative recombination in CRYRING. in *Dissociative Recombination of Molecular Ions with Electrons* (ed. Guberman, S. L.) (Kluwer Academic/Plenum, New York, in the press).
21. Plasil, R. *et al.* Advanced integrated stationary afterglow method for experimental study of recombination processes of H_3^+ and D_3^+ ions with electrons. *Int. J. Mass Spectrom.* **218,** 105–130 (2002).
22. Savage, B. D., Drake, J. F., Budich, W. & Bohlin, R. C. A survey of interstellar molecular hydrogen. I. *Astrophys. J.* **216,** 291–307 (1977).
23. Cardelli, J. A., Meyer, D. M., Jura, M. & Savage, B. D. The abundance of interstellar carbon. *Astrophys. J.* **467,** 334–340 (1996).
24. Bohlin, R. C., Savage, B. D. & Drake, J. F. A survey of interstellar H I from Lα absorption measurements. II. *Astrophys. J.* **224,** 132–142 (1978).
25. van Dishoeck, E. F. & Black, J. H. Comprehensive models of diffuse interstellar clouds — physical conditions and molecular abundances. *Astrophys. J. Suppl. Ser.* **62,** 109–145 (1986).
26. Lepp, S. in *Astrochemistry of Cosmic Phenomena* (ed. Singh, P. D.) 471–475 (IAU Symposium 150, Kluwer, Dordrecht, 1992).
27. Heiles, C. & Troland, T. H. The millennium Arecibo 21-cm absorption line survey. II. Properties of the warm and cold neutral media. *Astrophys. J.* (in the press); preprint astro-ph/0207105 at ⟨http://xxx.lanl.gov⟩ (2002).
28. Lindsay, C. M. & McCall, B. J. Comprehensive evaluation and compilation of H_3^+ spectroscopy. *J. Mol. Spectrosc.* **210,** 60–83 (2001).
29. Paul, J. B., Collier, C. P., Saykally, R. J., Scherer, J. J. & O'Keefe, A. Direct measurement of water cluster concentrations by infrared cavity ringdown laser absorption spectroscopy. *J. Phys. Chem. A* **101,** 5211–5214 (1997).

Acknowledgements B.J.M. and A.J.H. thank K. Wilson and C.-Y. Chung for their assistance in the laboratory, D. Lucas for the loan of equipment, and H. Chan and E. Granlund for their support. B.J.M. thanks T. Oka, L. M. Hobbs, D. G. York and T. P. Snow for conversations about the ζ Persei line of sight. We thank C. H. Greene for providing us with the results of his calculations in advance of publication. M.L. thanks D. Zajfman for information on TSR results before publication. The idea of using a supersonic expansion source for dissociative recombination measurements originated during conversations between B.J.M. and C. M. Lindsay, and the experiment was designed by B.J.M., A.J.H. and M.L. The supersonic expansion ion source was built and spectroscopically characterized by A.J.H. and B.J.M. in the laboratory of R.J.S. in Berkeley. The dissociative recombination measurements in Stockholm were carried out by all of the authors except R.J.S. and T.R.G. The UKIRT observations were obtained by B.J.M. and T.R.G. The authors thank the staff of the Manne Siegbahn Laboratory for help with the experiment. B.J.M. is supported by the Miller Institute for Basic Research in Science. A.J.H. and R.J.S. acknowledge support from the AFOSR and NSF. T.R.G. is supported by Gemini Observatory, operated by AURA for the international Gemini partnership. N.D. and G.H. were supported in part by the US DOE, Office of Fusion Energy. J.S. is supported in part by the State Committee for Scientific Research. Support is acknowledged from the EU fifth framework program, the EOARD, the Swedish Research Council and STINT.

Competing interests statement The authors declare that they have no competing financial interests.

Correspondence and requests for materials should be addressed to B.J.M. (e-mail: bjmccall@astro.berkeley.edu).

Structure and thermal history of the H-chondrite parent asteroid revealed by thermochronometry

Mario Trieloff*, Elmar K. Jessberger†, Ingrid Herrwerth‡, Jens Hopp*‡, Christine Fiéni§, Marianne Ghélis§, Michèle Bourot-Denise§ & Paul Pellas§||

** Mineralogisches Institut der Universität Heidelberg, Im Neuenheimer Feld 236, D-69120 Heidelberg, Germany*
† Institut für Planetologie, Westfälische Wilhelms-Universität, Wilhelm-Klemm-Straβe 10, D–48149 Münster, Germany
‡ Max-Planck-Institut für Kernphysik, Saupfercheckweg 1, D-69117 Heidelberg, Germany
§ Laboratoire de Minéralogie du Muséum, 61 rue Buffon, 75005 Paris, France
|| Deceased

Our Solar System formed ~4.6 billion years ago from the collapse of a dense core inside an interstellar molecular cloud. The subsequent formation of solid bodies took place rapidly. The period of <10 million years over which planetesimals were assembled can be investigated through the study of meteorites[1–3]. Although some planetesimals differentiated and formed metallic cores like the larger terrestrial planets, the parent bodies of undifferentiated chondritic meteorites experienced comparatively mild thermal metamorphism that was insufficient to separate metal from silicate[4,5]. There is debate about the nature of the heat source[6–9] as well as the structure and cooling

history of the parent bodies[10–12]. Here we report a study of ^{244}Pu fission-track and ^{40}Ar–^{39}Ar thermochronologies of unshocked H chondrites, which are presumed to have a common, single, parent body. We show that, after fast accretion, an internal heating source (most probably ^{26}Al decay[8–10,13]) resulted in a layered parent body[6] that cooled relatively undisturbed: rocks in the outer shells reached lower maximum metamorphic temperatures and cooled faster than the more recrystallized and chemically equilibrated rocks from the centre, which needed ~160 Myr to reach 390K.

The first condensation of refractory Ca–Al-rich inclusions (Allende CAIs) in the solar nebula occurred 4,566 ± 2 Myr ago[1,2]. Accretion and differentiation into silicate crust and metallic core of some asteroids was completed only a few million years later, as demonstrated by Pb–Pb ages of basaltic achondrites[3], whereas cooling of the iron cores extended over tens of millions of years[14]. In contrast, the cooling history and structure of the parent bodies of undifferentiated chondrites are not well established. Ordinary chondrites of one class (H, L or LL) share common properties such as oxygen isotopic composition, degree of iron oxidation and major element chemistry, suggesting a single parent body for each class. Moreover, each class can be subdivided into different petrologic types[4,5] that experienced specific degrees of thermal metamorphism: for example, type 6 chondrites were heated to higher metamorphic peak temperatures (~1,120 K) than those of type 4 (~920 K). A possible model for the early evolution of ordinary chondrite parent asteroids is an onion-shell-layered parent body (refs 6, 10) (Fig. 1). After accretion, the parent body consists of primitive material and is heated internally by decay energy of short-lived nuclides[8,9,13] such as ^{26}Al ($\tau_{1/2} = 0.72$ Myr). The outer shells lose heat more effectively, whereas the rocks in the centre are heated to higher metamorphic peak temperatures and cool down more slowly. However, as some studies did not show the expected correlation between metamorphic grade and cooling rate or age[15,16], other hypotheses were advanced that involve either separate parent bodies for each petrologic type[11] or early collisional fragmentation of an onion-shell-layered parent body, with final cooling in a 'rubble-pile' structure[12]. Moreover, alternative heat sources were considered (see review[7]), such as electric currents induced by an early, intense, solar-wind plasma.

Radiochronometry can elucidate the early parent asteroid evolution: in an onion-shell-layered parent body that cools undisturbed, type 6 chondrites cooled slower than type 4 chondrites. Slower cooling should result in lower cooling ages, as radiometric 'ages' actually represent cooling below a 'closure temperature' that is mineral specific, for example when Pb diffusion in phosphates becomes ineffective below ~720 K (refs 17–19), or when ^{40}Ar from ^{40}K decay is retained quantitatively in oligoclase feldspar below ~550 K (refs 19, 20). Other examples are ^{244}Pu-derived fission tracks stable in orthopyroxene below ~550 K (ref. 19) or in the phosphate merrillite below ~390 K (ref. 19). Most reliable

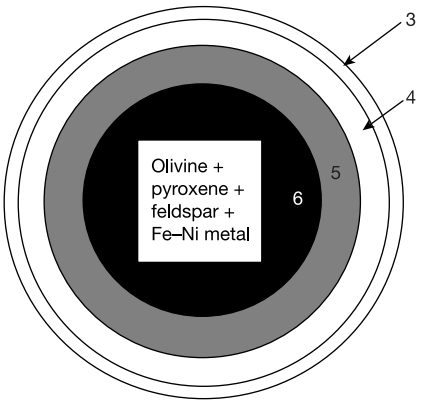

Figure 1 Onion-shell model for undifferentiated ordinary chondrite parent asteroids[6]. A celestial body that is internally heated (probably by the decay energy from short-lived ^{26}Al) reaches higher maximum metamorphic temperatures in its centre, resulting in higher petrologic types (numbers shown) that cool slower than in the outer layers, which in turn results in lower petrologic types with faster cooling. Increasing degrees of thermal metamorphism resulted, for example, in the extinction of primary chondrules, matrix recrystallization, formation of secondary feldspar and phosphates, and chemical equilibration of olivine and pyroxene. However, heating was insufficient for separation of metal and silicate and formation of an iron core.

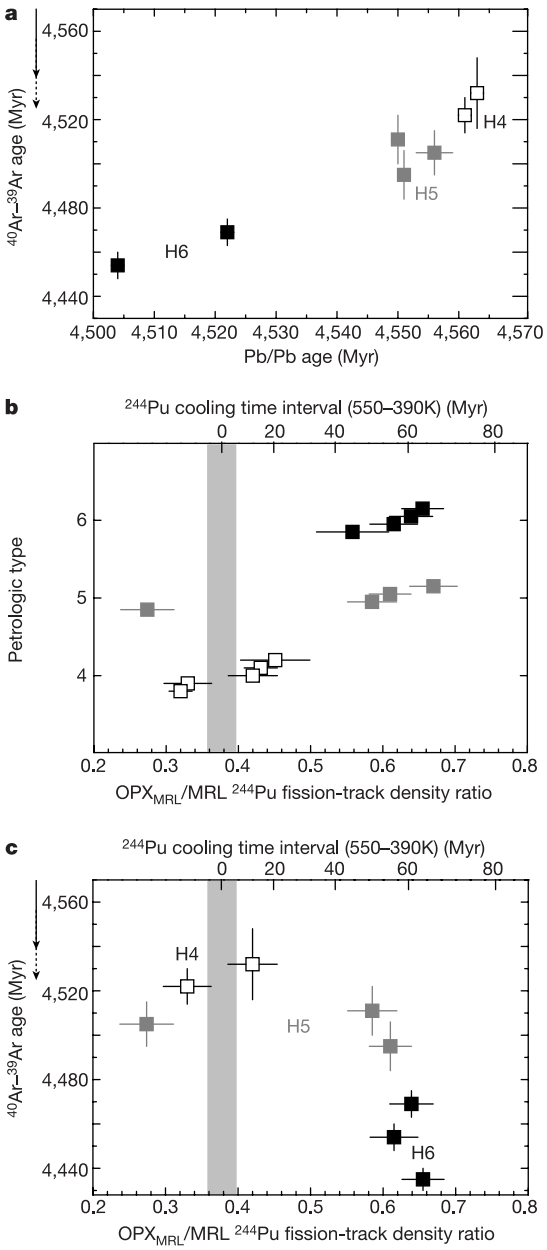

Figure 2 Correlation between cooling ages and metamorphic grade. **a**, Pb/Pb phosphate and ^{40}Ar–^{39}Ar feldspar cooling ages demonstrate that low petrographic types cooled faster to Pb closure in phosphates (~720 K) and Ar retention in feldspar (~550 K) than higher petrographic types. The arrow quantitatively indicates a possible shift of the K–Ar timescale caused by systematic error of the K decay constant, but note that age differences are not affected. **b**, Low petrographic types also cooled faster between 550 K and 390 K, as derived from cooling time intervals (upper scale) calculated from the ^{244}Pu fission-track density ratio (lower scale) in merrillite and adjacent orthopyroxene (see Supplementary Table S1). The systematic uncertainty of the ^{244}Pu timescale (induced by the normalization factor) is quantitatively shown by the grey band around zero. **c**, Correlation between ^{40}Ar–^{39}Ar feldspar cooling age and ^{244}Pu fission-track cooling time interval.

results are obtained when the different complementary methods (Pb–Pb, ^{40}Ar–^{39}Ar, ^{244}Pu fission tracks) are simultaneously applied to the aforementioned minerals that are major carriers of the parent nuclide. However, owing to the fine-grained nature of chondritic material, ^{40}Ar–^{39}Ar dating is commonly done on whole rocks[19,20]. Here we present the first combined feldspar, pyroxene and whole-rock ^{40}Ar–^{39}Ar data for ordinary chondrites (see Supplementary Figs S1–S6 and Table S2). We also present the first ^{244}Pu fission-track chronometric results that were evaluated with all-recent methodological improvements[19,21] (Supplementary Table S1). An indispensable requirement for obtaining information on the early parent-body history is to study exceptionally undisturbed chondrites. Only these preserve the earliest radiometric record from the period shortly after accretion, as they were not affected by secondary-impact-induced shock or reheating during the past ~4,000 Myr. Just a few unshocked H chondrites—like those we studied—satisfy this condition.

Table 1 provides a summary of ^{244}Pu fission-track, ^{40}Ar–^{39}Ar, and Pb–Pb chronometries of all H chondrites we studied, for which complete data sets are available now. The highest ages are Pb–Pb phosphate ages of H4 chondrites Forest Vale and Ste Marguerite. Obviously, accretion was complete 3.0 ± 2.6 Myr after Allende CAI formation 4,566 Myr ago (refs 1, 2, 18). H5 and H6 chondrites cooled progressively later below the Pb–Pb closure temperature. Our new results extend this trend to low-temperature chronometers: individual ^{40}Ar–^{39}Ar ages are generally lower than the respective Pb–Pb age (Table 1 and Fig. 2a). This can be interpreted as additional cooling time needed to reach ^{40}Ar retention in oligoclase feldspar at ~550 K. Moreover, high petrologic types needed a longer cooling time than low petrologic types, and reached isotopic closure later, leading to younger apparent ages. Slower cooling of H chondrites of high petrologic type is also confirmed by the cooling time intervals calculated from ^{244}Pu fission-track densities of orthopyroxene and merrillite, which register tracks at <550 and <390 K (Table 1). This correlation is also valid for other unshocked H chondrites for which, however, there are no complementary ^{40}Ar–^{39}Ar and Pb–Pb age data (Fig. 2b and Supplementary Table S1). Figure 2c shows that H5 and H6 chondrites, which needed longer for cooling to the Ar closure temperature of 550 K, also cooled more slowly afterwards until ^{244}Pu fission-track retention in merrillite at 390 K (except Nadiabondi).

Figure 3a displays integrated cooling curves: following the accretion shortly after 4,566 Myr (refs 1, 2), rapid heating resulted in different metamorphic peak temperatures, between 920 K and 1,120 K (ref. 5), at different depths. H4 Forest Vale and Ste Marguerite cooled down to the Pb closure temperature at 720 K within a few million years (4,561 and 4,563 Myr ago), whereas types H5 needed 10–16 Myr, and H6 Kernouve and Guarena considerably longer[18]. Subsequent cooling until ^{40}Ar retention in oligoclase at ~550 K needed additional time, and occurred later for H6 than for H5 and for H4. As ^{244}Pu fission tracks in orthopyroxene are also retained at ~550 K, ^{244}Pu cooling-time intervals until track registration in merrillite at ~390 K can thus be attached to the ^{40}Ar–^{39}Ar data: consequently H4 chondrites cooled to 390 K faster and earlier than H5 and H6 chondrites. Note that H6 Guarena, H6 Kernouve and H6 Estacado cooled slowly, but with significant differences, whereas the H5 Allegan and H5 Richardton have rather similar cooling histories. H4 Forest Vale and Ste Marguerite are also very similar, whereas H5 Nadiabondi seems to be intermediate between H5 and H4, as indicated by its Pb–Pb age and its steep ^{244}Pu fission-track cooling rate. Apparently, this H5 and the two H4 chondrites share a rather peculiar cooling history: fast cooling above 720 K and below 550 K seems to be interrupted by a slower cooling episode between 720 K and 550 K. However, this is most probably not significant, taking into account the recently suggested revision of the relative Pb–Pb and K–Ar age scales[22–25], resulting from the uncertainty in the K decay constant. A shift of the ^{40}Ar–^{39}Ar ages (and also ^{244}Pu ages) by 30 Myr (ref. 25) obviously provides a more concise explanation (Fig. 3b): then Ste Marguerite, Forest Vale and Nadiabondi cooled fast through the high- and low-temperature regimes, instead of having rather exotic 'fast–slow–fast' cooling histories. It is important to note that the K–Ar and ^{244}Pu age scales are shifted to the same degree, because the fission-track retention in orthopyroxene is linked to ^{40}Ar retention in feldspar. Although our data support the need for a revision of the K–Ar age scale, its exact magnitude[23–25] remains an issue.

We also present in Fig. 3b the modelled cooling curves at different depths of a chondritic asteroid 100 km in diameter that was heated

Table 1 **Summary of thermochronological data**

Meteorite	^{244}Pu fission track density ratio of orthopyroxene (merrillite contacts) and merrillite*	^{244}Pu cooling time interval† (Myr)	^{40}Ar–^{39}Ar age‡ relative to NL25 hornblende standard§ (Myr)	Pb–Pb age‖ (Myr)
Retention/closure temperature		550K (Opx), 390K (Mrl)	550 ± 20K (Oligoclase feldspar)	720 ± 50K (Phosphates)
H4				
Ste Marguerite	0.420 ± 0.034	12 ± 11	4,532 ± 16 WR	4,563 ± 1
Forest Vale	0.330 ± 0.033	<8 ¶	4,522 ± 8 WR	4,561 ± 1
H5				
Nadiabondi	0.261 ± 0.017	<−8 #	4,505 ± 10 WR, Px	4,556 ± 3
Richardton	0.610 ± 0.029	56 ± 9	4,495 ± 11 WR	4,551 ± 1
Allegan	0.585 ± 0.034	51 ± 9	4,511 ± 11 WR	4,550 ± 1
Sena	0.670 ± 0.033	66 ± 9		4,556 ± 1
H6				
Kernouve	0.639 ± 0.030	61 ± 8	4,469 ± 6 WR, Fs, Px	4,522 ± 1
Guarena	0.615 ± 0.033	56 ± 9	4,454 ± 6 WR, Fs, Px	4,504 ± 1
Estacado	0.655 ± 0.029	64 ± 8	4,435 ± 5 WR, Fs, Px	

*^{244}Pu fission-track densities in orthopyroxene (Opx) crystal surfaces that had been located adjacent to merrillite (Mrl) phosphate crystals; merrillite crystals were pre-annealed at 290 °C to erase cosmic-ray-induced spallation recoil tracks[19].

† The cooling time interval is obtained after correcting the fission-track densities for irradiation geometry and mineral registration efficiency. This correction factor induces an additional systematic uncertainty of the ^{244}Pu timescale, which need not be taken into account for comparison of relative cooling interval differences (see Methods).

‡ ^{40}Ar–^{39}Ar ages are error-weighted means of plateau ages of whole rock (WR), feldspar (Fs) and/or 'pyroxene' (Px) separates for H6 chondrites. Plateaux were also obtained for Nadiabondi WR and Forest Vale WR. For Richardton, Allegan and Ste Marguerite we calculated total ages (see Supplementary Figs S2 and S3). Note that in all chondrites feldspar is the dominant K-bearing and, hence, actually dated phase (see Methods and Supplementary Figs S1–S4). There is a very good agreement of ^{40}Ar–^{39}Ar ages obtained[20] on four of these H chondrites by using a different age monitor (see Supplementary Table S2).

§ Individual K–Ar ages were calculated by using the Steiger and Jäger[22] convention, and are calibrated against the age-standard NL25 hornblende[30] with a K–Ar age of 2,655 ± 9 Myr (see Supplementary Table S2). Uncertainties do not contain the systematic error due to the NL25-standard age error (a possible ±12 Myr shift of the ^{40}Ar–^{39}Ar age scale) and the K–decay constant uncertainty (an upward shift of ages of the order of 30–45 Myr)[23–25].

‖ Reference 18.

¶ Upper limit for cooling time interval at 2σ level.

Negative cooling time interval within 2σ uncertainties indicates fast cooling.

by ^{26}Al decay (with $^{26}Al/^{27}Al = 4 \times 10^{-6}$) 2.5 Myr after Allende CAI formation ($^{26}Al/^{27}Al = 5 \times 10^{-5}$) (ref. 8). We used the analytical model of Miyamoto *et al.*[10] (see Methods). Typical cooling curves provide good approximations to the measured cooling histories, with the H6 Estacado, H6 Guarena and H6 Kernouve being deepest and H4 Forest Vale and H4 Ste Marguerite (and possibly Nadiabondi) lying shallowest. It is apparent that this rather simple model not only provides general features like slower cooling in the centre and faster cooling near the surface, but also reproduces the non-exponential cooling paths of the H5 chondrites. Nevertheless, more refined models (for example, those that take into account effects of the slow development of insulating regolith layers that allow faster cooling in the low-temperature regime between 550 K and 390 K for the H4 chondrites) could probably provide even better fits to the data.

Our new results define the thermal history of the H-chondrite parent body to a much greater precision than previous studies not using rigorously unshocked or undisturbed samples[15] or mineral separates[16]. It agrees with the thermal history from I–Xe studies of chondritic mineral separates (ref. 26). It supports an internal heating mechanism, and favours decay energy of short-lived nuclides (for example ^{26}Al) as the planetesimal heat source in the early solar system[7,9,13]. Obviously, the interior regions cooled undisturbed down to 390 K, indicating that this parent body was not destroyed by early impacts. Fragmentation and re-assembly processes causing a rubble-pile structure of asteroids as currently observed[27] probably occurred much later. The early histories of other ordinary chondrite parent bodies remain to be assessed, but complementary radiometric data on mineral separates of unshocked L and LL chondrites with comparable precision are not yet available[11,15,18,20,26]. □

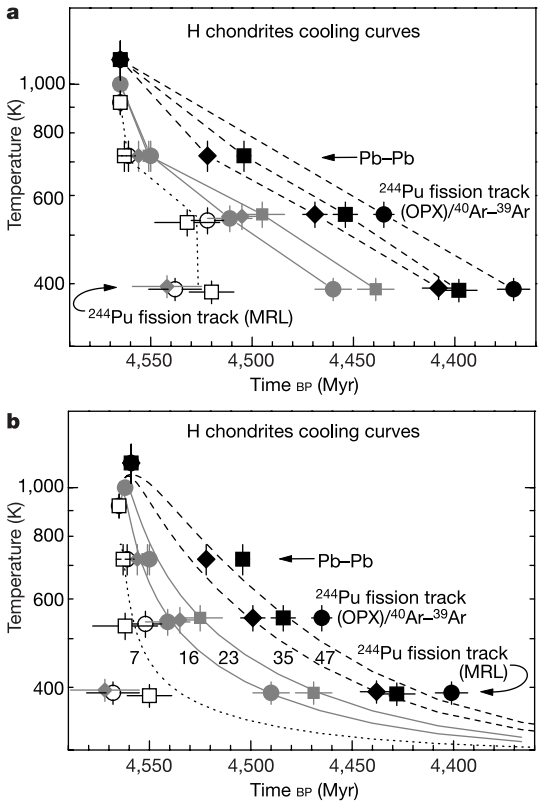

Figure 3 Integrated cooling curves for all H chondrites where complete chronological information is available. The Pb–Pb (at 720 K) and ^{40}Ar–^{39}Ar (at 550 K) cooling ages and ^{244}Pu fission track retention ages in orthopyroxene (OPX, at 550 K) and merrillite (MRL, at 390 K) are given. Low petrographic types cooled significantly faster than higher ones. **a**, ^{40}Ar–^{39}Ar ages as calculated after Steiger and Jäger[22]. Dashed lines: H6 Estacado (filled circles), Guarena (filled square), Kernouve (filled diamond). Solid lines: H5 Richardton (grey square), Allegan (grey circle), Nadiabondi (grey diamond). Dotted lines: H4 Forest Vale (open circle), Ste Marguerite (open square). **b**, Alternative hypothesis resulting from shifting ^{40}Ar–^{39}Ar and ^{244}Pu ages up by 30 Myr to account for recent suggestions to recalibrate the Pb/Pb and Ar–Ar age scales[23–25]. The cooling curves are calculated for a chondritic 100-km diameter asteroid that is internally heated by ^{26}Al decay for depths of 47, 35 (dashed), 23, 16 (solid) and 7 km (dotted). Symbols as in **a**.

Methods

Sample selection

Investigating the earliest parent-body history 4,600 Myr ago requires samples that were unaffected by impact-induced shock or heating during the past 4,000 Myr. Thus we applied three criteria to select our samples: (1) absence of shock features (see Supplementary Table S1); (2) presence of ^{244}Pu fission tracks—short-lived ^{244}Pu produces detectable tracks only >4,000 Myr ago, and subsequent reheating to >390 K is excluded because annealing temperatures (in merrillite) are low; (3) absence of major disturbances of the Pb–Pb system in phosphates. Additional studies of even only moderately shocked H4 chondrites (Ochansk, Menow; Supplementary Fig. S3c) revealed irregularities and inconclusive chronological results that simulate complex parent-body histories.

^{244}Pu fission-track thermochronometry

Short-lived ^{244}Pu ($\tau_{1/2} = 80$ Myr) is concentrated in the phosphates apatite and merrillite. Spontaneous ^{244}Pu fission leaves radiation damage visible by etching as fission tracks. These are also registered by accidentally adjacent silicate minerals[28]. Upon cooling below a certain temperature, radiation damage is no longer annealed and fission tracks are retained, for example in orthopyroxene below ~550 K and in merrillite below ~390 K (ref. 19). If—appropriately corrected[19]—the fission-track densities in both minerals are the same, 'instantaneous' fast cooling is indicated, whereas a fission-track density ratio of 2 corresponds to a cooling time interval of 80 Myr at an average rate of 2 K Myr^{-1}. Important major corrections to fission-track dating introduced in recent years are (1) erasure of cosmic-ray-induced spallation recoil tracks in phosphates by crystal tempering at 290 °C (refs 19, 21), and (2) correction for different mineral-specific registration efficiencies. The more effective track registration in merrillite compared with that in orthopyroxene results in an effective correction factor of 1.325 ± 0.074 (average of previously used values[19,21]) for the orthopyroxene/merrillite fission-track density ratio. To account for the irradiation geometry an additional factor of 2 has to be included. To check for relative cooling histories of meteorites, that is, cooling time interval differences, it is, however, appropriate to compare the uncorrected ratios (Table 1 and Fig. 2b, c). This is because the systematic uncertainties of the registration efficiency factor need not be included, which is the case when calculating absolute ^{244}Pu cooling-time intervals (Table 1 and Fig. 2b, c).

^{40}Ar–^{39}Ar cooling ages

In ^{40}Ar–^{39}Ar dating we studied whole rock samples, but also feldspar and pyroxene mineral separates of H6 chondrites, where thermal metamorphism had led to growth of large (>50 μm) grains of secondary feldspar[4,5]. All 15 samples were analysed with high resolution (up to 42 heating steps), crucial for obtaining the spectral fine structure. The spectra (Table 1, and Supplementary Table S2 and Figs S1–S3) exclude significant secondary ^{40}Ar losses. However, those of the low petrologic-type chondrites are somewhat disturbed by ^{39}Ar recoil as expected for fine-grained mineral assemblages. The fine structures of such age spectra that are disturbed by ^{39}Ar recoil, but which still exhibit intermediate age plateaux, have previously been modelled quantitatively[29]. It was demonstrated that the plateau segments yield reliable age information whereas the ages from initial and final extractions are to be discarded. As is evident from the K/Ca ratio spectra and the release patterns of K-derived ^{39}Ar and Ca-derived ^{37}Ar (Supplementary Figs S1–S4), the chronological information of whole rock samples is controlled by the main K carrier, oligoclase feldspar. Even in pyroxene mineral separates analysed by us, most K was located in fine-grained feldspar impurities that were not successfully separated (Supplementary Figs S1, S2 and S4). This is consistent with our observation of no significant age difference between whole rock, feldspar and pyroxene separates (Table 1 and Supplementary Figs S1 and S2 and Table S2). Accordingly, the average ^{40}Ar–^{39}Ar age calculated from these different plateau ages from a single H chondrite can be directly interpreted as the feldspar cooling age. To minimize relative uncertainties, all samples were calibrated against the same NL25 age standard[30]. Ages were calculated by using the convention of Steiger and Jäger[22], but a recalibration of the relative K–Ar and Pb–Pb age scales should be considered[23–25] (see main text). For irradiation details, see Supplementary Table S2 and Fig. S6.

Parent body heating model

In the calculation of the cooling curves of material in a chondritic parent body that is heated by the decay of ^{26}Al (Fig. 2b), we applied the analytical model of Miyamoto *et al.*[10]. As in ref. 10 our parameters are thermal conductivity (1.0 W mK^{-1}), density (3.2 g cm^{-3}), heat generation (11.67 × $^{26}Al/^{27}Al$ W m^{-3}) and emissivity. We slightly adapted the radius (100 instead of 85 km), accretion temperature T_0 (300 instead of 200 K), and initial $^{26}Al/^{27}Al$ ratio (4×10^{-6} instead of 5×10^{-6}). This $^{26}Al/^{27}Al$ ratio is a factor of 12.5 lower than in CAIs and corresponds to H chondrite accretion 2.5 Myr after the formation of Allende CAIs. It is in agreement with the Pb–Pb age difference of CAIs of 4,566 Myr and Ste Marguerite of 4,563 Myr (refs 1, 2, 18).

Received 13 December 2002; accepted 18 February 2003; doi:10.1038/nature01499.

1. Chen, J. H. & Wasserburg, G. J. The isotopic composition of uranium and lead in Allende inclusions and meteoritic phosphates. *Earth Planet. Sci. Lett.* **5,** 15–21 (1981).
2. Allègre, C. J., Manhès, G. & Göpel, C. The age of the Earth. *Geochim. Cosmochim. Acta* **59,** 1445–1456 (1995).
3. Lugmair, G. W. & Galer, S. J. G. Age and isotopic relationships among the angrites Lewis Cliff 86010 and Angra dos Reis. *Geochim. Cosmochim. Acta* **56,** 1673–1694 (1992).
4. van Schmus, W. R. & Wood, J. A. A chemical-petrologic classification for the chondritic meteorites. *Geochim. Cosmochim. Acta* **31,** 747–765 (1967).
5. Dodd, R. T. Metamorphism of the ordinary chondrites: a review. *Geochim. Cosmochim. Acta* **33,** 161–203 (1969).
6. Herndon, J. M. & Herndon, M. A. Aluminium-26 as a planetoid heat source in the early solar system. *Meteoritics* **12,** 459–465 (1977).
7. Wood, J. A. & Pellas, P. in *The Sun in Time* (eds Sonett, C. P., Giampapa, M. S. & Matthews, M. S.) 741–760 (Univ. of Arizona Press, Tucson, 1991).
8. Lee, T., Papanastassiou, D. A. & Wasserburg, G. W. Demonstration of ^{26}Mg excess in Allende and evidence for ^{26}Al. *Geophys. Res. Lett.* **3,** 109–112 (1976).
9. Knodlseder, J., Cervino, M., Le Duigou, J. M., Meynet, G., Schaerer, D. & von Ballmoos, P. Gamma-ray line emission from OB associations and young open clusters–II. The Cygnus region. *Astron. Astrophys.* **390,** 945–960 (2002).
10. Miyamoto, M., Fujii, N. & Takeda, H. Ordinary chondrite parent body: an internal heating model. In *Proc. Lunar Planet. Sci. Conf.* **12B,** 1145–1152 (1981).
11. Scott, E. R. D. & Rajan, R. S. Metallic minerals, thermal histories and parent bodies of some xenolithic, ordinary chondrite meteorites. *Geochim. Cosmochim. Acta* **45,** 53–67 (1981).
12. Grimm, R. E. Penecontemporaneous metamorphism, fragmentation, and reassembly of ordinary chondrite parent bodies. *J. Geophys. Res.* **90**(B2), 2022–2028 (1985).
13. Zinner, E. & Göpel, C. Aluminum-26 in H4 chondrites: implications for its production and its usefulness as a fine-scale chronometer for early solar system events. *Meteoritics Planet. Sci.* **37,** 1001–1013 (2002).
14. Wood, J. A. The cooling rates and parent planets of several iron meteorites. *Icarus* **3,** 429–459 (1964).
15. Taylor, G. J., Maggiore, P., Scott, E. R. D., Rubin, A. E. & Keil, K. Original structures, and fragmentation and reassembly histories of asteroids: evidence from meteorites. *Icarus* **69,** 1–13 (1987).
16. Jordan, J., Kirsten, T. & Richter, H. ^{129}I/^{127}I: a puzzling early solar system chronometer. *Z. Naturforsch.* **35**(a), 145–170 (1980).
17. Cherniak, D., Lanford, W. A. & Ryerson, F. J. Lead diffusion in apatite and zircon using ion implantation and Rutherford backscattering techniques. *Geochim. Cosmochim. Acta* **55,** 1663–1673 (1991).
18. Göpel, C., Manhès, G. & Allègre, C. J. U–Pb systematics of phosphates from equilibrated ordinary chondrites. *Earth Planet. Sci. Lett.* **121,** 153–171 (1994).
19. Pellas, P., Fieni, C., Trieloff, M. & Jessberger, E. K. The cooling history of the Acapulco meteorite as recorded by the ^{244}Pu and ^{40}Ar–^{39}Ar chronometers. *Geochim. Cosmochim. Acta* **61,** 3477–3501 (1997).
20. Turner, G., Enright, M. C. & Cadogan, P. H. The early history of chondrite parent bodies inferred from ^{40}Ar–^{39}Ar ages. *Proc. Lunar Planet. Sci. Conf.* **9,** 989–1025 (1978).
21. Lavielle, B., Marti, K., Pellas, P. & Perron, C. Search for extinct ^{248}Cm in the early Solar System. *Meteoritics* **27,** 382–386 (1992).
22. Steiger, R. H. & Jäger, E. Subcommission on Geochronology: convention on the use of decay constants in geo- and cosmochronology. *Earth Planet. Sci. Lett.* **36,** 359–362 (1977).
23. Renne, P. R. ^{40}Ar/^{39}Ar age of plagioclase from Acapulco meteorite and the problem of systematic errors in cosmochronology. *Earth Planet. Sci. Lett.* **175,** 13–26 (2000).
24. Begemann, F. *et al.* Call for an improved set of decay constants for geochronological use. *Geochim. Cosmochim. Acta* **65,** 111–121 (2001).
25. Trieloff, M., Jessberger, E. K. & Fiéni, C. Comment on '^{40}Ar/^{39}Ar age of plagioclase from Acapulco meteorite and the problem of systematic errors in cosmochronology' by Paul R. Renne. *Earth Planet. Sci. Lett.* **190,** 267–269 (2001).
26. Brazzle, R. H., Pravdivtseva, O. V., Meshik, A. P. & Hohenberg, C. M. Verification and interpretation of the I–Xe chronometer. *Geochim. Cosmochim. Acta* **63,** 739–760 (1999).
27. Pravec, P. & Harris, A. W. Fast and slow rotation of asteroids. *Icarus* **148,** 12–20 (2000).
28. Pellas, P. & Storzer, D. Mesures des taux de refroidissement des chondrites ordinaires à partir des traces de fission du plutonium 244 enregistrées dans les cristaux détecteurs. *C. R. Acad. Sci. III D* **280,** 225–228 (1975).
29. Trieloff, M., Deutsch, A. & Jessberger, E. K. The age of the Kara impact structure, Russia. *Meteoritics Planet. Sci.* **33,** 361–372 (1998).
30. Schaeffer, G. A. & Schaeffer, O. A. ^{40}Ar–^{39}Ar ages of lunar rocks. *Proc. Lunar Planet. Sci. Conf.* **8,** 2253–2300 (1977).

Supplementary Information accompanies the paper on *Nature*'s website (http://www.nature.com/nature).

Acknowledgements We thank B. Dominik for mineral separation, A. Bouikine and E. Korotchantseva for assisting in ^{40}Ar–^{39}Ar analyses, and D. Stöffler for shock-stage classification of some H chondrites. We appreciate discussions with J.A. Wood, E. Anders and T. Althaus, and support from R. Altherr, T. Kirsten and K. Mauersberger at various stages of this study. M.T., E.K.J. and J.H. acknowledge support from the Deutsche Forschungsgemeinschaft.

Author contributions P.P. provided the motivation for this research by his enthusiastic work on ^{244}Pu fission-track studies.

Competing interests statement The authors declare that they have no competing financial interests.

Correspondence and requests for materials should be addressed to M.T. (e-mail: trieloff@min.uni-heidelberg.de).

Critical thickness for ferroelectricity in perovskite ultrathin films

Javier Junquera & Philippe Ghosez

Département de Physique, Université de Liège, Bâtiment B-5, B-4000 Sart-Tilman, Belgium

The integration of ferroelectric oxide films into microelectronic devices[1,2], combined with the size reduction constraints imposed by the semiconductor industry, have revived interest in the old question concerning the possible existence of a critical thickness for ferroelectricity. Current experimental techniques have allowed the detection of ferroelectricity in perovskite films down to a thickness of 40 Å (ten unit cells), ref. 3. Recent atomistic simulations[4,5] have confirmed the possibility of retaining the ferroelectric ground state at ultralow thicknesses, and suggest the absence of a critical size. Here we report first-principles calculations on a realistic ferroelectric–electrode interface. We show that, contrary to current thought, $BaTiO_3$ thin films between two metallic $SrRuO_3$ electrodes in short circuit lose their ferroelectric properties below a critical thickness of about six unit cells (~24 Å). A depolarizing electrostatic field, caused by dipoles at the ferroelectric–metal interfaces, is the reason for the disappearance of the ferroelectric instability. Our results suggest the existence of a lower limit for the thickness of useful ferroelectric layers in electronic devices.

Epitaxial growth of high-quality thin films of ABO_3 perovskite oxides on semiconductors—Si (ref. 6) and Ge (ref. 1)—and metallic[7] substrates has opened the door to the use of alternative materials in metal-oxide-semiconductor field-effect transistors (MOSFETs)[1,8] and non-volatile ferroelectric random access memories (FERAMs)[9,10]. Recently, 30 Gbit cm^{-2} data storage densities have been demonstrated for $Pb(Zr_{0.2}Ti_{0.8})O_3$ films on a metallic oxide electrode[2]. As the size of high-quality perovskite layers of interest for technological applications decreases, the fundamental questions of the thickness dependence of the ferroelectric properties, and of their possible disappearance at a finite critical thickness, become crucial.

It was thought that ferroelectricity was suppressed in small particles and thin films[11], but this situation changed after experiments that identified ferroelectric ground states in 40-Å-thick perovskite oxide films[3] and in 10-Å-thick crystalline copolymer films[12]. In support of these experimental observations, theoretical investigations using a phenomenological approach[13], first-principles effective hamiltonian calculations[4] and full first-principles simulations[5] predicted ferroelectric ground states for various ABO_3 slabs under the condition of vanishing internal electric field. However, in all these approaches, the influence of a real metal–perovskite interface (including the finite screening length of the electrode, the interface chemistry and the strain conditions imposed by the substrate) on both the atomic relaxation and polarization was missing—or was only empirically included through the choice of specific electromechanical boundary conditions. The only more-fundamental study of metal–$BaTiO_3$ interfaces is due to Rao *et al.*[14], but does not address the question of the ferroelectric instability.

Here we simulate from first principles the behaviour of a typical ferroelectric capacitor structure epitaxially grown on a thick $SrTiO_3$ substrate, and made of an ultrathin film of $BaTiO_3$ (a prototypical ferroelectric oxide) between two metallic $SrRuO_3$ electrodes[15] (Fig. 1). The electrical boundary conditions are fixed by putting the electrodes in short-circuit. Calculations were done within density functional theory and the local density approximation.

